SWIFT-XRT-CALDB-09

Release Date: 2013-Dec-20

Prepared by: Andrew Beardmore[1], Julian Osborne[1], Claudio Pagani[1], Sergio Campana[2]

Document revision date: 2014-Jan-17

Revision: 18

Revised by: Andrew Beardmore

Affiliation: [1] University of Leicester, [2] INAF-OAB

SWIFT XRT CALDB RELEASE NOTE

SWIFT-XRT-CALDB-09:

Response matrices and Ancillary Response Files

Table P1: Files to be released:

Filename	Mode	Grade	Substrate† voltage (V)	Release Date
swxwt0to2s6_20010101v015.rmf	WT	$0-2$	6	2013-Dec-20
swxwt0s6_20010101v015.rmf	WT	0	6	2013-Dec-20
swxpc0to12s6_20010101v014.rmf	PC	$0-12$	6	2013-Dec-20
swxpc0to4s6_20010101v014.rmf	PC	$0-4$	6	2013-Dec-20
swxpc0s6_20010101v014.rmf	PC	0	6	2013-Dec-20
swxs6_20010101v001.arf*	PC & WT	–	6	2013-Dec-20

† The substrate voltage was permanently raised from $V_{ss} = 0\,\mathrm{V}$ to $V_{ss} = 6\,\mathrm{V}$ on 2007-Aug-30 (see below).

* Unified ARF for both WT and PC modes.

Scope of Document

This document describes the release of updated *Swift*-XRT Windowed Timing (WT) and Photon Counting (PC) mode redistribution matrix files (RMFs) and ancillary response file (ARF), appropriate for data taken after the CCD substrate voltage change on 2007-Aug-30 — i.e. for $V_{ss} = 6\,\mathrm{V}$ data (see table P1).

Introduction

The XRT effective area is made up of three main components: the mirror effective area, the filter transmission and the CCD quantum efficiency (QE). The QE is included directly in the redistribution matrix files (RMFs) while the ancillary response files (ARFs) contain the mirror effective area and the filter transmission.

Observation-specific ARF files are produced by the XRTMKARF task (part of the XRTDAS-HEADAS software). This task corrects the nominal (on-axis, infinite extraction region) ARF file from the CALDB for the effects of telescope vignetting and, optionally (*psfflag=yes*), for PSF losses incurred when finite sized extraction regions are used in point source analysis. Additional corrections for CCD defects (caused by 'bad columns' or 'hot-pixels') can be made with the inclusion of an exposure map (with the option *expofile=filename.img*), which can automatically be generated by the data analysis pipeline. The task can also generate ARFs for extended sources (option *extended=yes*), such as clusters of galaxies or supernova remnants.

As well as accounting for the CCD QE, the RMFs model the response of the detector to incident X-rays and are mode, grade and epoch dependent.

Epoch Dependent RMFs

The XRT suffered a thermoelectric cooler power supply failure shortly after launch which meant the CCD could not be operated at the expected nominal temperature of $-100\,^{\circ}\mathrm{C}$. However, by carefully controlling the spacecraft pointing during pre-planned science observations the CCD can be passively cooled to acceptable temperatures in the range ~ -75 to $-50\,^{\circ}\mathrm{C}$ (Kennea et al. 2005, SPIE, 5898, 329).

Furthermore, laboratory testing showed that by raising the CCD substrate voltage from $V_{ss} = 0\,\mathrm{V}$ to $V_{ss} = 6\,\mathrm{V}$ the thermally induced dark current in the CCD could be reduced, allowing the CCD to operate a few degrees warmer before excessive hot pixels compromise data quality and telemetry (Godet et al., 2009, A&A, 494, 775). Because of this, the XRT CCD substrate voltage was permanently raised to $V_{ss} = 6\,\mathrm{V}$ on 2007-Aug-30 (at 14:28UT).

A side effect of increasing the substrate voltage in this way is that it caused the CCD depletion depth to decrease slightly which, in turn, altered the QE at high energies and just below the Si edge ($\sim 1.5 - 1.84\,\mathrm{keV}$). This warranted the release of response calibration files specific to the different substrate operating voltages.

Over time, the accumulated radiation dose and high-energy proton interactions cause damage to the CCD (in the imaging area, the store frame area and the serial register) resulting in a build-up of charge traps (i.e. faults in the Si crystalline structure of the CCD which hold onto some of the charge released during an X-ray interaction). The deepest traps are responsible for the strongest line FWHM degradation, with the line shape then showing a more pronounced low energy wing. The most serious of these charge traps can cause a loss of up to $\sim 600\,\mathrm{eV}$ at $6\,\mathrm{keV}$ and $\sim 300\,\mathrm{eV}$ at $1.856\,\mathrm{keV}$ from the incident X-ray energy, although typical values are very much smaller.

For observations taken on or after 2007-Sep-01, we have mapped the location and depths of the deepest traps on the CCD and updated the *Swift*-XRT XRTCALCPI software task to provide a trap specific energy scale reconstruction (see the gain file release note SWIFT-XRT-CALDB-04_v10 and later for details and caveats). The application of such trap corrections help to restore the spectral resolution (FWHM) of the detector — improvements in FWHM from 180 eV in PC (225 eV in WT) at 1.86 keV in early 2009 to approximately 135 eV (for both modes) are seen. By 2013, the trap corrected FWHM at 1.86 keV had increased to 150 eV in PC mode and 170 eV in WT mode.

Both the change in substrate voltage and degredation in spectral resolution (up to the point at which trap corrections have been enabled) necessitate the release of RMFs with different QEs and kernel broadening depending on the epoch of the observation.

Motivation behind this release

This release provides new WT and PC mode RMFs generated by the recently improved CCD22 modelling code, first introduced in the CALDB release of 2013-Mar-13 (described in SWIFT-XRT-CALDB-09_v17), but now updated for $V_{ss} = 6\,\mathrm{V}$ observations. This release also makes available a grade $0-4$ RMF in PC mode for the first time.

It also provides an updated ARF, derived from new mirror area file computations (including the effects of a thin hydrocarbon coating) and optical blocking filter transmission curve modelling. This ARF is now identical to the one described in SWIFT-XRT-CALDB-09_v17 and we refer the reader to that document for further information concerning its creation.

RMF/ARF file naming scheme

The change in substrate voltage made it necessary to release two sets of RMF/ARF files, distinguished by the characters 's0' and 's6' in their filenames. The filenames also encode the XRT readout mode (WT or PC), the grade selection ($0-2$ or 0 for WT; $0-12$, $0-4$ or 0 for PC) and the epoch the files are valid for use from.

The RMFs released this time are, for WT mode:

swxwt0to2s6_20010101v015.rmf	**grade** $0-2$
swxwt0s6_20010101v015.rmf	**grade** 0

and for PC mode :

swxpc0to12s6_20010101v014.rmf	**grade** $0-12$
swxpc0to4s6_20010101v014.rmf	**grade** $0-4$
swxpc0s6_20010101v014.rmf	**grade** 0

(Note, whilst all scientifically interesting $V_{ss} = 6\,\mathrm{V}$ data were taken after the permanent switch to $V_{ss} = 6\,\mathrm{V}$ operation on 2007-Aug-30, the filename epoch predates this to account for the small amount of $V_{ss} = 6\,\mathrm{V}$ calibration data taken for testing purposes before the substrate voltage change was made permanent.)

A common ARF is now available, valid for both modes, all grade selections and throughout the $V_{ss} = 6\,\mathrm{V}$ epoch :

swxs6_20010101v001.arf

The files announced here supersede the $V_{ss} = 6\,\mathrm{V}$ v013 PC RMF/ARFs and the v014 WT RMF/ARFs released on 2011-Jul-25 (described in release note SWIFT-XRT-CALDB-09_v16).

The RMFs are located in the HEASARC CALDB under the directory $CALDB/data/swift/xrt/cpf/rmf and the ARF under $CALDB/data/swift/xrt/cpf/arf.

A complete summary of all RMFs/ARFs presently in use can be found in table A1.

Updated $V_{ss} = 6\,\mathrm{V}$ Redistribution Matrix Files

The *Swift*-XRT X-ray detector is a CCD22 device produced by e2v and is the same type of CCD used in the *XMM-Newton* EPIC MOS cameras. The CCD Response Matrix Files (RMFs) are created by a newly rewritten Monte-Carlo simulation code (Beardmore 2014 in prep.). Godet et al. (2009, A&A, 494, 775 and references therein), described the previous version of the code, though many of the details written there are still applicable to the new code. The improvements made to the CCD simulation code with respect to the old version were highlighted in the 2013-Mar-13 RMF release document (SWIFT-XRT-CALDB-09_v17), which was applicable for $V_{ss} = 0\,\mathrm{V}$ observations.

In order to refine the CCD simulator code input parameters and produce RMFs appropriate for $V_{ss} = 6\,\mathrm{V}$ observations we made use of PC mode data taken from the internal Fe-55 calibration source, as well as calibration observations of astrophysical sources taken in both PC and WT mode.

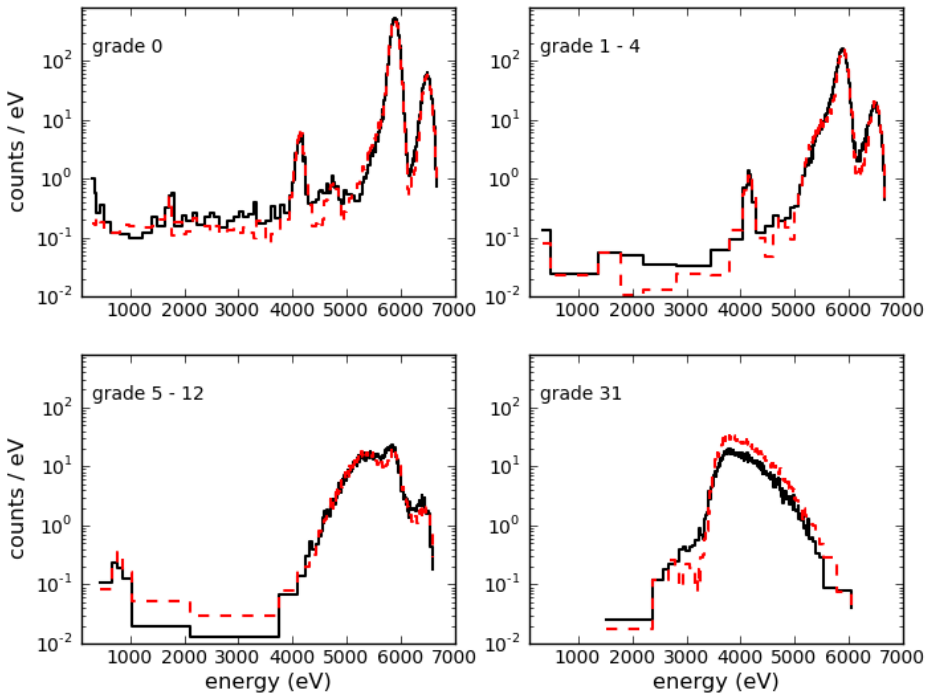

Figure 1: Corner source 3, trap-free, Fe-55 spectra taken during 2008 as a function of grade (black) along with the CCD simulator model (red).

The slight reduction in QE caused by operating the CCD at $V_{ss} = 6\,\mathrm{V}$ was modelled in the CCD simulator by using a mean depletion depth of 19.4 microns, compared with 27 microns for the $V_{ss} = 0\,\mathrm{V}$ case. The initial post-substrate voltage change response broadening was modelled assuming a electronic noise of $7.5\,e^-$ and serial/parallel CTI of 3.5×10^{-5}.

Trap free PC mode data taken from the Fe-55 corner source closest to the readout node (i.e. corner source 3 at $DETX, DETY = 38, 27$, extending to a radius of 50 pixels) during 2008 is shown in figure 1 (in black) as a function of grade. The modelled response (in red) agrees very well with the data and shows that the instrument response kernel is quite broad for grades > 4 (as these events are primarily produced by X-rays which interact deeply in the Silicon in the field-free region). For this reason we have released an additional grade $0-4$ RMF for PC mode this time, which benefits from having an energy resolution intermediate between that of grade 0 (170 eV) and grade $0-12$ (180 eV) at 6 keV, while having 90% of the grade $0-12$ QE.

Comparison with Calibration data

A number of astrophysical sources were used to verify the XRT calibration and check the level of agreement seen between other X-ray observatories, some results from which follow.

SNR 1E0102.2–7219

Observations of the low-energy, line-rich source SNR 1E0102.2–7219 from 2008-Aug/Oct were used, along with its IACHEC reference model (Plucinsky et al., 2012, SPIE, 8443, 12), to refine the intrinsic resolution of the response kernel in both PC and WT mode at this time (see figure 2).

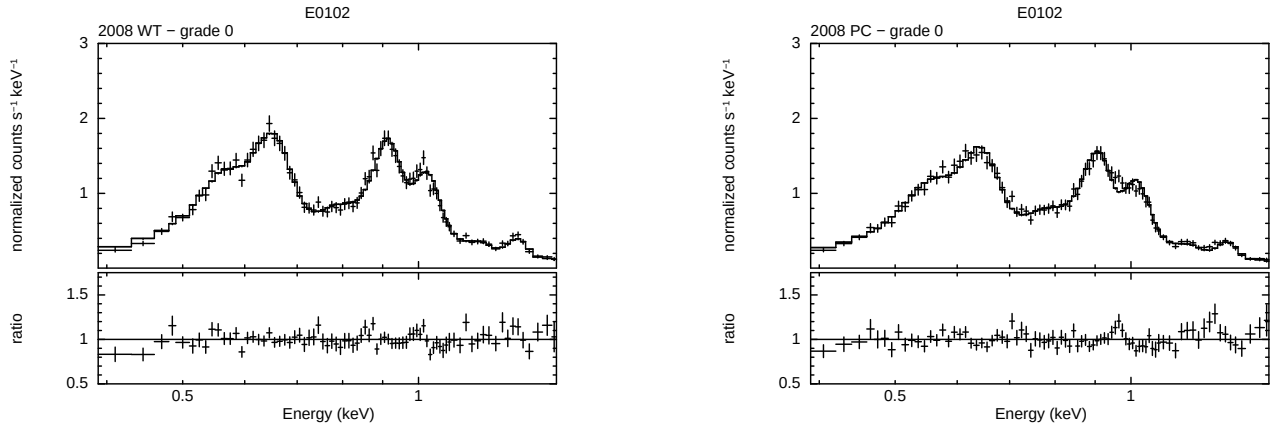

Figure 2: SNR 1E0102.2–7219 WT (left) and PC (right) spectra (both grade 0) from 2008-Aug/Oct, modelled using the IACHEC reference model and the latest response files described in this document, illustrating the good agreement of the observed and modelled low energy spectral resolution at this epoch.

RX J1856.5–3754

The isolated neutron star RX J1856.5–3754 is considered to be a stable, soft X-ray source, modelled as a 63 eV blackbody (e.g. Beuermann et al., 2006, A&A, 458, 541). The source has been observed regularly since the substrate voltage changed in order to monitor the low energy response of the XRT.

The relative normalisation of the model when applied to grade 0 data from different observational epochs and as a function of the lowest energy used in the fit is shown in table 1.

Table 1: Fits to the relative blackbody normalisation (assuming a temperature of 63 eV) to epoch dependent $V_{ss} = 6$ V WT and PC mode grade 0 spectra as a function of the fit lower energy.

	WT mode				PC mode			
Year	Ontime	Fit lower energy (keV)			Ontime	Fit lower energy (keV)		
	(ks)	0.30	0.35	0.40	(ks)	0.30	0.35	0.40
2007	47.7	0.922 ± 0.021	0.965 ± 0.025	0.984 ± 0.029	40.1	0.804 ± 0.019	0.813 ± 0.024	0.834 ± 0.028
2008	78.0	0.944 ± 0.017	0.994 ± 0.020	1.033 ± 0.024	79.7	0.782 ± 0.013	0.810 ± 0.017	0.822 ± 0.019
2009	27.9	0.852 ± 0.028	0.966 ± 0.035	1.002 ± 0.040	18.3	0.781 ± 0.029	0.831 ± 0.036	0.862 ± 0.043
2010	41.6	0.885 ± 0.024	0.935 ± 0.028	0.956 ± 0.033	38.4	0.741 ± 0.019	0.750 ± 0.024	0.772 ± 0.028
2011	39.2	0.850 ± 0.027	0.925 ± 0.032	0.958 ± 0.037	39.7	0.765 ± 0.019	0.782 ± 0.023	0.821 ± 0.028
2012	37.4	0.820 ± 0.028	0.912 ± 0.033	0.908 ± 0.037	39.7	0.786 ± 0.019	0.812 ± 0.024	0.842 ± 0.028
2013	20.3	0.776 ± 0.033	0.865 ± 0.041	0.879 ± 0.047	17.7	0.777 ± 0.029	0.798 ± 0.036	0.830 ± 0.042

(with uncertainties calculated at $\Delta C = 2.7$ (90% confidence) level). For comparison, shortly after launch in 2005, the relative normalisation were 1.08 ± 0.08 for WT and 0.90 ± 0.05 for PC.

For both modes, the relative normalisation is seen to slowly decrease with time when fitting the data down to 0.3 keV, with WT mode, in particular, showing a loss of low energy counts with time below ~ 0.4 keV (see figure 3).

The loss of low energy counts is related to a build up of charge traps within the CCD, as traps cause a significant fraction of charge from low energy X-rays to be lost below the event threshold, which is then not recoverable. For unabsorbed sources such as this, the effect can be alleviated by increasing the lowest energy used in the fit — for example, to 0.4 keV in 2013.

PKS 0745–19

The galaxy cluster PKS 0745–19 has been observed by the XRT on multiple occasions and is a suitable source for checking the relative PC mode calibration before and after the substrate voltage change was made. The data

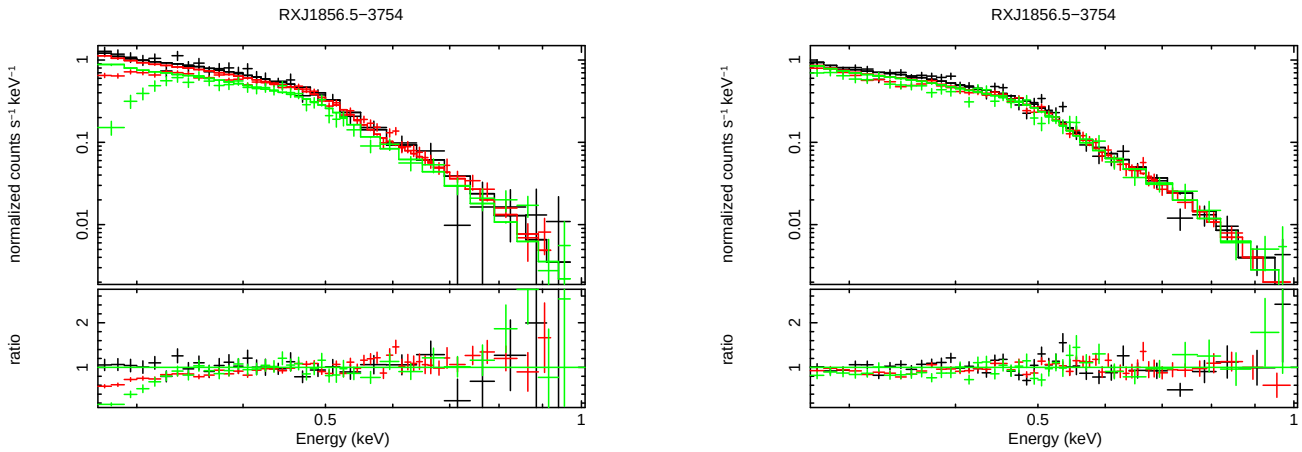

Figure 3: RX J1856.5–3754 WT (left) and PC (right) spectra (both grade 0) from 2005 (black), 2008 (red) and 2013 (green) and modelled with a 63 eV blackbody. The WT spectra show a drop-off in counts at the lowest energies with time due to the build-up of charge traps.

were analysed in two epochs, before and after the substrate voltage change, with spectra extracted from a region containing the central 90 arcseconds of the cluster core (to maximise the signal to noise), using the XRT pointings made within 3 arcminutes of the cluster centre (to reduce the effects of vignetting) and extended source ARFs were generated. The results (see table 2 and figure 4(a)) show wideband fluxes, temperatures and column densities which are in good agreement between the different substrate voltage epochs.

Table 2: XRT PC mode fits to spectra from the central 60 arcsecs of the galaxy cluster PKS 0745–19. $V_{ss} = 0$ V data are included for comparison. The assumed model is TBABS*APEC (with xsect vern and abund wilm). The uncertainties were calculated at the $\Delta C = 1$ level.

Epoch	Ontime (ks)	V_{ss}[a]	Grade	NH[b]	kT[c]	Flux[d]
2005	57.7	0	$0-12$	5.44 ± 0.12	7.50 ± 0.30	4.08 ± 0.03
			0	5.45 ± 0.14	7.54 ± 0.34	4.14 ± 0.03
2007–2012	115.9	6	$0-12$	5.71 ± 0.10	7.57 ± 0.23	4.04 ± 0.02
			$0-4$	5.66 ± 0.10	7.47 ± 0.24	4.01 ± 0.02
			0	5.66 ± 0.10	7.19 ± 0.27	3.96 ± 0.02

[a] Substrate voltage; [b] Column density from TBABS ($\times 10^{21}$ cm^{-2}); [c] APEC temperature (keV); [d] $0.3-8.0$ keV observed flux ($\times 10^{-11}$ erg cm^{-2} s^{-1}).

SNR G21.5–0.9

The heavily absorbed powerlaw source SNR G21.5–0.9 is regularly observed in PC mode for calibration purposes and it was used to refine the post-substrate voltage change QE at high energies. The results from spectral fits to the accumulated post-substrate voltage data (containing $> 10^5$ counts in 238 ks) are shown in table 3 and figure 4(b) for different grades.

The fits show excellent agreement with the pre-substrate voltage change data (whose grade $0-12$ spectra were fit with a column density of $3.13 \pm 0.09 \times 10^{22}$ cm^{-2}, a photon index of 1.87 ± 0.04 and a $2-8$ keV unabsorbed flux of $5.52 \pm 0.07 \times 10^{-11}$ erg cm^{-2} s^{-1}), and with the cross-calibration comparison of Tsujimoto et al. (2011, A&A, 525, A25).

We note the high S/N dataset used here show a ~ 10 percent residual around the Si edge in the grade 0 spectrum, which drops to 5 percent in grade 0–12 (see figure 4(b)).

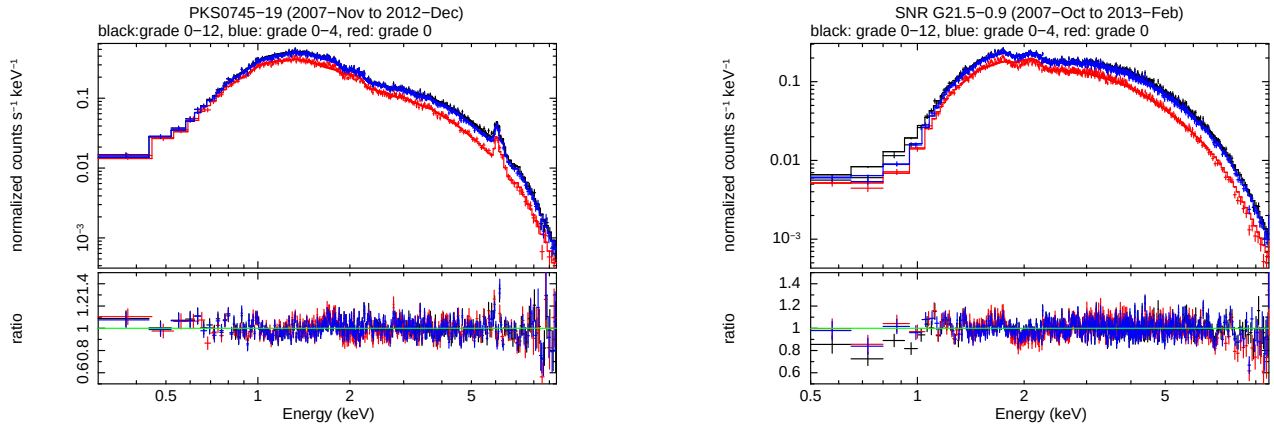

Figure 4: $V_{ss} = 6$ V PC mode spectral fitting results. Left (a): the intermediately absorbed PKS 0745–19. Right (b): the heavily absorbed SNR G21.5–0.9. The colours refer to grade $0-12$ (black), grade $0-4$ (blue) and grade 0 (red).

Table 3: $V_{ss} = 6$ V PC mode spectral fit results for SNR G21.5–0.9. The assumed model is TBABS*PEGPWRLW (with xsect vern and abund wilm). The uncertainties were calculated at the $\Delta C = 1$ level.

Grade	NH^a	Γ^b	Norm^c
$0-12$	3.25 ± 0.02	1.87 ± 0.01	5.69 ± 0.02
$0-4$	3.22 ± 0.02	1.87 ± 0.01	5.63 ± 0.02
0	3.08 ± 0.03	1.86 ± 0.01	5.37 ± 0.02

^{a} Column density from TBABS ($\times 10^{21}$ cm^{-2}); ^{b} Powerlaw photon index, Γ; ^{c} Powerlaw normalisation, which is the $2.0-8.0$ keV unabsorbed flux ($\times 10^{-11}$ erg cm^{-2} s^{-1}).

PKS 2155–304

PKS 2155–304 was observed on 2008-May-12 in both PC mode and WT mode — the 3 snapshots of the latter were taken between 8 snapshots of the former. As the source was at a count rate of 7 count s^{-1}, an annulus from $17-30$ pixels (radius) was used to avoid pile-up in the PC data. While the light curve showed a ~ 15 per cent variation through the observations, a hardness ratio suggested the source was spectrally stable, hence the data were used to check the inter-mode calibration. The results of powerlaw fits (see table 4) show good agreement between the modes with photon indices which differ by only 0.10 ± 0.07.

Table 4: XRT WT and PC mode observations of PKS 2155–304 taken on 2008-May-12. The spectra are modelled with TBABS*POWERLAW) over $0.35-9$ keV (with xsect vern and abund wilm). The uncertainties were calculated at the $\Delta C = 1$ level.

Mode	Ontime (ks)	Grade	NH^a	Γ^b	Flux^c
WT	5.0	0-2	1.9 ± 0.5	2.52 ± 0.03	1.70 ± 0.02
		0		2.50 ± 0.03	1.72 ± 0.02
PC	11.2	0-12	1.3 ± 1.0	2.40 ± 0.06	1.92 ± 0.06
		0-4		2.40 ± 0.06	1.93 ± 0.06
		0		2.41 ± 0.07	1.92 ± 0.07

^{a} Column density ($\times 10^{20}$ cm^{-2}), tied between grades. (C.f. expected galactic column density of 1.6×10^{20} cm^{-2}); ^{b} Powerlaw photon index, Γ; ^{c} Observed flux over $0.35-9.0$ keV ($\times 10^{-10}$ erg cm^{-2} s^{-1}) — note the source was temporally variable at the level of 15 percent on the day of the observations.

On 2013-Apr-24 the XRT performed a cross-calibration observation of PKS 2155–304 simultaneously with XMM,

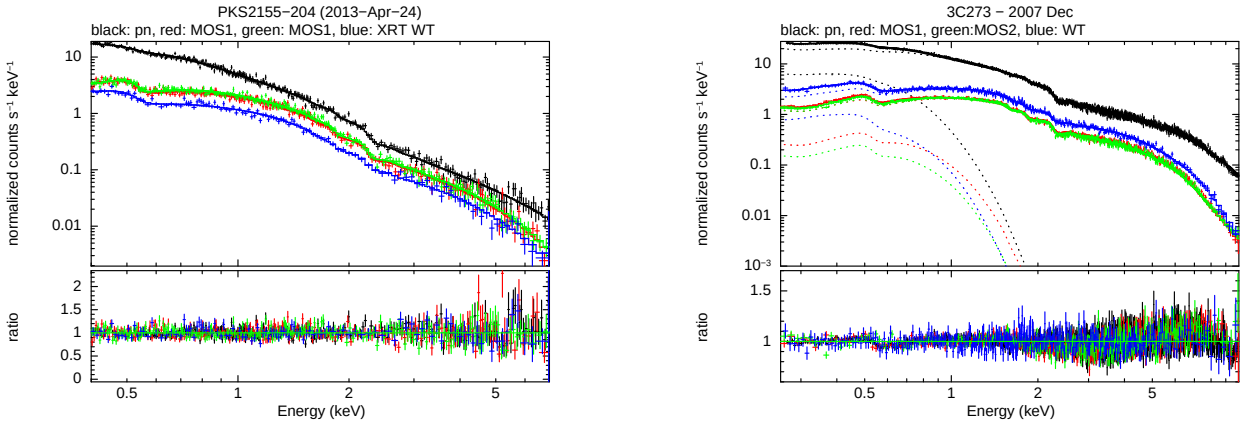

Figure 5: Spectral fit comparisons. Left (a): absorbed powerlaw fits to PKS 2155–304 data taken in 2013-Apr-24 (table 5) showing *XMM-Newton* pn (black), MOS1 (red), MOS2 (green) and XRT WT (grade $0-2$) (blue). Right (b): absorbed (powerlaw + zbbody) fits to 3C 273 data taken on 2007-Dec-08 (table 6), showing *XMM-Newton* pn (black), MOS1 (red), MOS2 (green) and XRT WT (grade $0-2$) (blue).

Chandra and NuStar. The results from XMM and XRT (during which the XRT was in WT mode for an exposure of 7.7ks) are given in table 5 (see figure 5(a)) and show excellent agreement between the two instruments.

Table 5: Cross-calibration results from simultaneous XRT WT and *XMM-Newton* EPIC observations of PKS 2155–304 taken on 2013-Apr-24. The spectra are modelled with TBABS*POWERLAW) over $0.4-7\,\mathrm{keV}$ (with xsect vern and abund wilm). The uncertainties were calculated at the $\Delta C = 1$ level.

Instr	NH[a]	Photon index	Flux[b]
pn	1.9 ± 0.4	2.76 ± 0.02	4.55 ± 0.03
MOS1	2.8 ± 0.5	2.77 ± 0.03	4.81 ± 0.04
MOS2	3.5 ± 0.5	2.81 ± 0.02	4.92 ± 0.04
WT g0-2	2.8 ± 0.7	2.69 ± 0.03	4.55 ± 0.05
WT g0	2.8 ± 0.7	2.68 ± 0.04	4.60 ± 0.05

[a] Column density ($\times 10^{20}\,\mathrm{cm}^{-2}$) (C.f. expected galactic (HI) column density of $1.6 \times 10^{20}\,\mathrm{cm}^{-2}$); [b] Observed flux over $0.4-7.0\,\mathrm{keV}$ ($\times 10^{-11}\,\mathrm{erg\,cm}^{-2}\,\mathrm{s}^{-1}$).

3C 273

XRT WT observations of the quasar 3C 273 were taken contemporaneously with *XMM-Newton* on 2007-Dec-08. Spectral comparisons were made over $0.3-10.0\,\mathrm{keV}$ and are shown in table 6 and figure 5(b). The results again show good agreement between the spectral parameters and fluxes consistent to better than 10 per cent.

Current limitations and future prospects

Experience has shown that the RMF/ARFs described here can be used reliably over the energy range $0.3(0.4^1) - 10\,\mathrm{keV}$ in PC mode and $0.3(0.4^1) - 10\,\mathrm{keV}$ in WT mode and return fluxes which agree to within better than 10 per cent when compared with other X-ray missions.

The following considerations apply when using the RMFs/ARFs described here:

[1] Depending on the epoch (see below).

Table 6: Cross-calibration results from 3C 273 comparing XRT WT and *XMM-Newton* EPIC observations obtained on 2007-Dec-08. The spectra are modelled with TBABS*(POWERLAW + ZBBODY) over $0.3-10\,\mathrm{keV}$ (with xsect vern and abund wilm). The uncertainties were calculated at the $\Delta C = 1$ level.

Instr	NH[a]	Photon index	$\mathrm{kT_{bb}}$[b]	Flux[c]
pn	< 0.1	1.612 ± 0.004	0.127 ± 0.002	3.06 ± 0.01
MOS1	< 0.1	1.611 ± 0.007	0.141 ± 0.006	3.12 ± 0.02
MOS2	< 0.2	1.661 ± 0.008	0.134 ± 0.010	3.44 ± 0.02
WT g0-2	2.1 ± 0.6	1.559 ± 0.013	0.113 ± 0.007	3.25 ± 0.05
WT g0	2.3 ± 0.6	1.559 ± 0.014	0.110 ± 0.007	3.30 ± 0.05

[a] Column density ($\times 10^{20}\,\mathrm{cm^{-2}}$) (C.f. expected galactic column density of $1.7 \times 10^{20}\,\mathrm{cm^{-2}}$); [b] Blackbody temperature (keV); [c] Observed flux over $0.3-10.0\,\mathrm{keV}$ ($\times 10^{-10}\,\mathrm{erg\,cm^{-2}\,s^{-1}}$).

- The loss function, which is used by the simulator to describe how charge is incompletely collected from the X-ray interactions occurring near the surface of the device, shifts the redistribution peak of the lowest energy data down in energy. The loss function was derived from pre-launch laboratory calibration data obtained at the University of Leicester, using the central 200×200 pixel region of the detector, in order to be representative of XRT pointings taken close to the on-axis position. At the lowest input energies (C-Kα at 0.277 keV; N-Kα at 0.392 keV), the redistribution is seen to be non-uniform (see figure 6). If a source is positioned outside the central 200×200 region then it might show slightly worse redistribution than modelled by the RMF at the lowest energies (below $\sim 0.4\,\mathrm{keV}$).

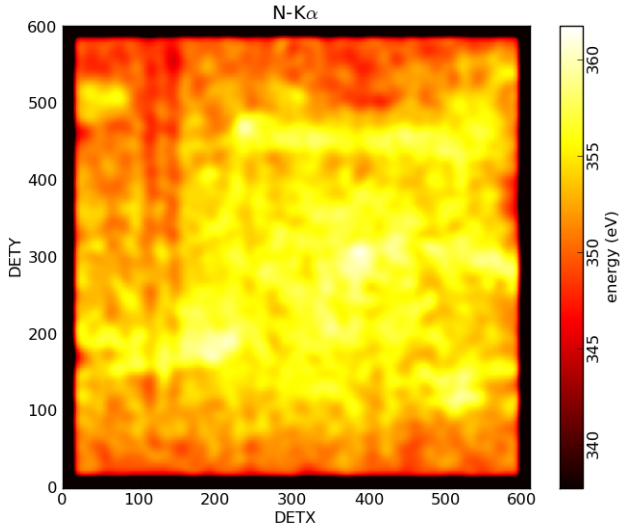

Figure 6: The spatial non-uniformity in the XRT spectral response over the surface of the detector at energies below $\sim 0.4\,\mathrm{keV}$ is illustrated in this image which shows the average event energy for N-Kα (0.392 keV) photons obtained from pre-launch laboratory calibration data. Event energy shifts of order $10-15\,\mathrm{eV}$ are visible outside the central 200×200 pixel region (from within which the response matrix loss function is calculated).

- The event threshold was fixed at 80DN onboard shortly after launch. However, in terms of energy, the effective threshold has increased slowly with time as the build up of traps has caused an evolution in the gain. For example, in WT mode, the effective threshold increased from $\sim 250\,\mathrm{eV}$ in 2007-Sep (shortly after the substrate voltage changed) to $\sim 320\,\mathrm{eV}$ by 2013-Nov. As the traps appear shallower in PC mode, the effective threshold has only increased from $\sim 240\,\mathrm{eV}$ to $\sim 280\,\mathrm{eV}$ in this mode over the same time.

  The XRT team are evaluating the prospect of decreasing the onboard event threshold in order to provide data which can once more be used down to 0.3 keV. In the meantime, users should be aware that spectra from unabsorbed sources taken since $\sim 2011-2012$ can only be reliably fit down to $\sim 0.35-0.4\,\mathrm{keV}$.

- High signal-to-noise WT spectra from sources with featureless continua (such as Mrk 421) typically show residuals of about 3 per cent, for example, near the Au-$\mathrm{M_V}$ edge (at 2.205 keV), the Si-K edge (at 1.839 keV), or the O-K edge (at 0.545 keV). Occasionally, however, residuals nearer the 10 per cent level are seen, especially near the O-K edge, which are caused by small energy scale offsets (caused by inaccurate bias and/or gain corrections).

  Data taken in PC mode can be similarly effected, though observations taken in this mode tend to have fewer counts and hence a lower statistical quality, which make the residuals less apparent.

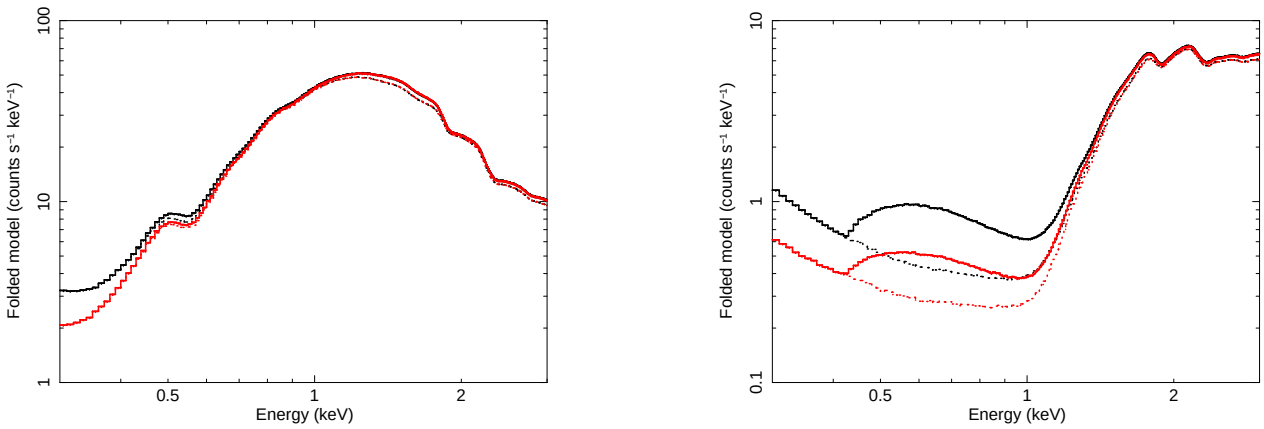

Figure 7: WT simulations of a point source, assuming a $\Gamma = 2$ powerlaw incident spectrum absorbed by 5×10^{21} atoms cm^{-2}, on the left, and 5×10^{22} atoms cm^{-2}, on the right. The black spectra are appropriate for a source located on a WT 10-row binning boundary (in this case at DETY=300.5), while the red spectra are for a source positioned 5 pixels away from the 10-row binning boundary (DETY=305.5). Solid curves show grade $0-2$ and dotted curves grade 0. (Note, the grade 0 and grade $0-2$ spectra are almost identical in the left panel.)

Such residuals can often be improved through careful use of the *gain* command in XSPEC (by allowing the gain offset to vary by $\sim \pm 10 - 50$ eV).

- Simulations of WT spectra using a point source illumination model reveal that the redistribution level is dependent on the location of the source on the CCD, as illustrated in figure 7 — a source positioned directly on a 10-row binning boundary experiences a higher fraction of event splitting, which gives rise to slightly heavier redistribution, than one whose vertical position is offset by a few pixels. Differences in the simulated redistribution levels become apparent for column densities above a few $\times 10^{21}$ cm^{-2}. Furthermore, the effect is found to be dependent on the event threshold, with a higher threshold causing more events in the redistribution tail and a grade $1-2$ redistribution bump (seen between $0.6-1$ keV) which shifts to higher energies.

  The new WT RMFs released here are created assuming the CCD is uniformly illuminated by X-rays at a threshold appropriate for the early $V_{SS} = 6$ V epoch. This means there is the potential for slight under (or over) estimates of the redistributed spectrum towards low energies, depending on the position of the source on the detector, epoch of the observation and level of absorption seen in the spectrum.

  We plan to evaluate the possibility of releasing source position dependent WT RMFs in the future.

- Trap-corrected XRT spectra show a slow broadening of the energy resolution with time. The energy resolution of the RMFs released here were matched to data taken in 2008/2009. We plan to release further broadened $V_{ss} = 6$ V RMFs spanning ~ 3 year intervals in the future.

Summary of RMFs/ARFs currently in use

The following table summarises the RMFs and ARFs available and recommended for XRT spectral analysis and their time dependence.

Table A1: *Swift*-XRT RMFs/ARFs in use as of 2013-Dec-20.

Observation Date		Mode	Grade	File names
From	To			
2004-Dec-01	2006-Dec-31	WT	0-2	swxwt0to2s0_20010101v012.rmf swxs0_20010101v001.arf
			0	swxwt0s0_20010101v012.rmf swxs0_20010101v001.arf
		PC	0-12	swxpc0to12s0_20010101v012.rmf swxs0_20010101v001.arf
			0	swxpc0s0_20010101v012.rmf swxs0_20010101v001.arf
2007-Jan-01	2007-Aug-30	WT	0-2	swxwt0to2s0_20070101v012.rmf swxs0_20010101v001.arf
			0	swxwt0s0_20070101v012.rmf swxs0_20010101v001.arf
		PC	0-12	swxpc0to12s0_20070101v012.rmf swxs0_20010101v001.arf
			0	swxpc0s0_20070101v012.rmf swxs0_20010101v001.arf
Substrate voltage change from 0 V to 6 V on 2007-August-30				
2007-Aug-31	present	WT	0-2	swxwt0to2s6_20010101v015.rmf swxs6_20010101v001.arf
			0	swxwt0s6_20010101v015.rmf swxs6_20010101v001.arf
		PC	0-12	swxpc0to12s6_20010101v014.rmf swxs6_20010101v001.arf
			0-4	swxpc0to4s6_20010101v014.rmf swxs6_20010101v001.arf
			0	swxpc0s6_20010101v014.rmf swxs6_20010101v001.arf

Note, the task XRTMKARF automatically reads in the correct ARF from the CALDB, based on information concerning the mode, grade and time of observation contained in the header of the input spectral file. The task also indicates to the screen which RMF is appropriate for the spectrum.

Useful Links

Summary of XRT RMF/ARF releases	http://www.swift.ac.uk/Gain_RMF_releases.html
XRT analysis at GSFC	http://swift.gsfc.nasa.gov/docs/swift/analysis
XRT analysis threads at the UKSSDC, University of Leicester	http://www.swift.ac.uk/XRT.shtml
XRT digest pages at the UKSSDC, University of Leicester	http://www.swift.ac.uk/xrtdigest.shtml
IACHEC website	http://web.mit.edu/iachec/